ChemComm

COMMUNICATION

View Article Online
View Journal | View Issue

Cite this: *Chem. Commun.*, 2015, 51, 10479

Received 12th May 2015,
Accepted 26th May 2015

DOI: 10.1039/c5cc03946k

www.rsc.org/chemcomm

(Fe,Co)@nitrogen-doped graphitic carbon nanocubes derived from polydopamine-encapsulated metal–organic frameworks as a highly stable and selective non-precious oxygen reduction electrocatalyst†

Jiangbo Xi,‡ Yating Xia,‡ Yangyang Xu, Junwu Xiao* and Shuai Wang*

A facile approach is reported to synthesize (Fe,Co)@nitrogen-doped graphitic carbon (NGC) nanocubes (NCs) *via* the pyrolysis of polydopamine-encapsulated $Fe_3[Co(CN)_6]_2$ NCs at 700 °C. Besides the comparable catalytic activity for oxygen reduction reaction (ORR) to the Pt/C catalyst, it showed much more outstanding catalytic selectivity and superior durability.

Recently, to replace precious metal (Pt,Pd) catalysts, numerous efforts have been made to explore highly efficient non-precious catalysts for the sluggish oxygen reduction reaction (ORR), including, for example, transition metal compounds,[1] Fe_3C,[2–4] metal-free doped carbon materials,[5,6] N-coordinated metal on carbon matrices (M–N–C, M = Co, Fe, Ni, *etc.*),[7] and even conducting polymers.[8] Among them, M–N–C catalysts are believed to be some of the most promising non-precious catalysts owing to their low cost and desirable catalytic activity. The different structures of M–N–C catalysts have been developed by pyrolizing appropriate precursors with nitrogen, carbon, and transition metallic ions.[9] However, structural and component control is still difficult to form highly efficient catalysts.

As a sub-class of metal–organic frameworks (MOFs), Prussian blue analogues (PBA), with the chemical formula $M_3^{II}[M^{III}(CN)_6]_2$, are created by the supramolecular assembly of transition metal cations with N-containing organic ligands. Therefore, they are believed to be promising precursors to prepare M–N–C catalysts with the controllable component and structure. The catalysts derived from PBA nanocrystals have been reported to exhibit good ORR catalytic activity.[2,10,11] The carbon supports, such as Vulcan XC-72 and graphene, adsorbed at the surface of the catalysts mainly improve the electrical conductivity, thus enhancing the catalytic activity. By contrast, transition metallic nanoparticles embedded by carbon materials, such as carbon nanotubes (CNTs) and graphitic shells, not only improve the electron transport characteristics, but also change the local work function, resulting in enhanced ORR activity and improved cycle life.[4,12] Moreover, introducing the nitrogen atom into carbon structure can induce charge delocalization to enhance ORR activity.[5] However, nitrogen-doped carbon materials have been rarely studied for encapsulating transition metallic nanoparticles, not to mention nitrogen-doped carbon in the crystalline state.

The nitrogen-doped carbon matrices were usually formed by the chemical vapor deposition (CVD) process in the presence of nitrogen sources and the pyrolysis of appropriately selected nitrogen-containing organic precursors. The CVD process is often too tedious and expensive for mass production, and the nitrogen sources, such as NH_3 and N_2H_4, are generally corrosive and toxic. The bottleneck associated with the pyrolysis of organic precursors lies in the high temperature process (~1000 °C) and low electric conductivity of carbon matrices due to poor crystallinity. Polydopamine (PDA) composed of cross-linked indole quinone units easily sticks to the surface of all types of solid materials regardless of their chemical nature, and can be pyrolyzed into highly conductive carbon film. The conductivity of up to 1200 S cm^{-1} can be achieved, which is comparable to that of polycrystalline graphite (1250 S cm^{-1})[13] and much higher than that of reduced graphene oxide (*e.g.* 727 S cm^{-1}, 1100 °C)[14] and pyrolyzed polycyclic aromatic hydrocarbon (206 S cm^{-1}, 1100 °C).[15]

Here we report a facile approach to synthesize a new type of ORR catalyst based on core–shell (Fe,Co)@NGC NCs *via* the one-step pyrolysis of PDA-encapsulated $Fe_3[Co(CN)_6]_2$ NC precursors at a low temperature (700 °C). Owing to its unique structure and component, besides high catalytic activity, the (Fe,Co)@NGC NCs catalyst exhibits excellent selectivity and stability. The fabrication process for the (Fe,Co)@NGC NCs is schematically depicted in Fig. 1A. The $M_3[M'(CN)_6]_2$ (M, M′ = Fe, Co) NCs were initially formed *via* a precipitation reaction between M^{2+} cations and $[M'(CN)_6]^{3-}$ anions in the presence of PVP. After being immersed in an aqueous solution of dopamine, a thin adherent PDA would be spontaneously anchored on the surface of $M_3[M'(CN)_6]_2$ to form $M_3[M'(CN)_6]_2$@PDA NCs (Stage I

Key Laboratory for Large-Format Battery Materials and System, Ministry of Education, Department of Chemistry and Chemical Engineering, Huazhong University of Science & Technology, Wuhan, P. R. China.
E-mail: chjwxiao@hust.edu.cn, chmsamuel@hust.edu.cn

† Electronic supplementary information (ESI) available. See DOI: 10.1039/c5cc03946k

‡ They contribute equally to this work.

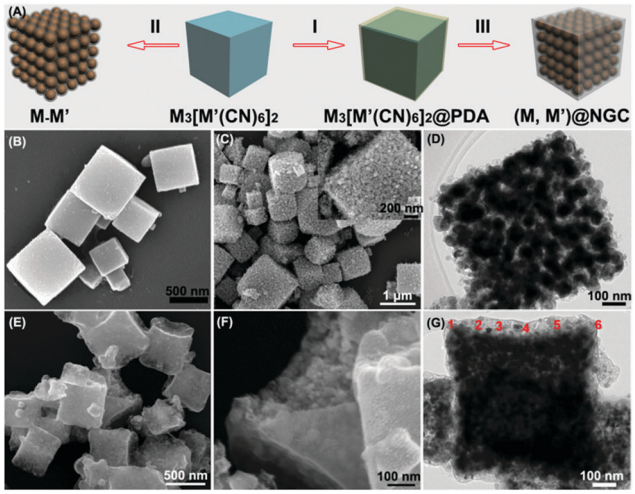

Fig. 1 (A) Schematic graph of the formation process of the (M, M′)@nitrogen-doped graphitic carbon (NGC) NCs. (B) SEM image of the $Fe_3[Co(CN)_6]_2$ NCs. (C, D) SEM and TEM images of the (Fe,Co) NCs (inset: high magnification SEM image). (E–G) SEM and TEM images of the (Fe,Co)@NGC NCs.

in Fig. 1A). The $M_3[M'(CN)_6]_2$ and $M_3[M'(CN)_6]_2$@PDA NCs were finally decomposed into the (M, M′) and (M, M′)@NGC NCs, respectively (Stages II and III in Fig. 1A).

The typical morphology and microstructure of the products are examined by electron microscopy, and the results are shown in Fig. 1B–G. The $Co_3[Co(CN)_6]_2$ and $Fe_3[Co(CN)_6]_2$ NCs with smooth surfaces are formed (Fig. 1B, Fig. S1A, S2B and C, ESI†), as Co^{2+} and Fe^{2+} cations are added into $[Co(CN)_6]^{3-}$ anions in the presence of PVP, respectively. Analogously, the $Fe_4[Fe(CN)_6]_3$ NCs are formed *via* a hydrothermal process of $K_4Fe(CN)_6$ (Fig. S1B and S2A, ESI†). $Fe_3[Co(CN)_6]_2$ NCs can be pyrolyzed into (Fe,Co) with the conserved nanocube morphology in the temperature range of 600–900 °C (Fig. 1C and Fig. S3, ESI†). The high magnification SEM and TEM images show that the (Fe,Co) NCs have coarse surface and porous structure, and are composed of numerous nanoparticles (inset of Fig. 1C and D). Such features are favourable for electrolyte filling and rapid transport. The formation of a porous structure is due to the weight loss during the pyrolysis process, according to the TGA results (Fig. S4, ESI†). The TGA curve of the $Fe_3[Co(CN)_6]_2$ NCs reveals two decomposition processes: (i) the first weight loss between 30 and 150 °C is attributed to the loss of water molecules;[2] (ii) the second weight loss is observed between 150 and 450 °C, ascribed to the decomposition of the cyanide ligand.[16] After depositing the PDA layer on the $Fe_3[Co(CN)_6]_2$ NCs, the cyanide ligand and PDA are completely degraded at over 600 °C. Further inspection using high-resolution TEM (HRTEM) shows that only a few (Fe,Co) nanoparticles are encapsulated by the graphitic layer (Fig. S5A and B, ESI†). When the $Fe_3[Co(CN)_6]_2$ NCs were immersed in a buffer solution of dopamine, dopamine was self-polymerized at the surface of $Fe_3[Co(CN)_6]_2$ NCs to form $Fe_3[Co(CN)_6]_2$@PDA NCs. The $Fe_3[Co(CN)_6]_2$@PDA NCs are transformed into (Fe,Co)@C NCs *via* a similar calcination process at 700 °C under an Ar atmosphere (Fig. 1E). The core–shell structure can be clearly seen from Fig. 1F and G. The carbon shell was further investigated by HRTEM, as shown in Fig. S6 (ESI†). It is found that the carbon sources come from the cyanide ligand and PDA has been successfully pyrolyzed into the graphitic carbon rather than amorphous carbon, which should be ascribed to the catalysis of Fe and Co.[2,17] Upon pyrolysis at 700 °C under an Ar atmosphere, the $Co_3[Co(CN)_6]_2$ and $Fe_4[Fe(CN)_6]_2$ NC precursors were transformed into Co and Fe, respectively (Fig. S7, ESI†).

XPS measurements were conducted to elucidate the chemical composition and nitrogen bonding configuration in the (Fe,Co) and (Fe,Co)@NGC NCs. The survey XPS spectra of the (Fe,Co) and (Fe,Co)@NGC NCs reveal the presence of C, N, O, Fe, and Co elements (Fig. S8A, ESI†). The C 1s spectrum is fitted according to the following carbon bonding environments: 284.5 (C–C), 286.5 (C–N/C–OH), 289.3 (O═C–O), and 292.7 eV (π–π* shake up).[18] The π–π* shake up peak in the (Fe,Co) and (Fe,Co)@NGC NCs reveals that carbon is with the aromatic characteristics of graphitic structure.[19] The N 1s XPS spectrum can be de-convoluted into three peaks with the binding energies of ~398.1, 399.4 and 401.4 eV, corresponding to pyridinic, pyrrolic, and graphitic N atoms, respectively (Fig. 2B). Among them, the graphitic N atom is dominant, with a percentage of 37.9% for (Fe,Co) NCs and 56.1% for (Fe,Co)@NGC NCs. The O 1s spectrum corresponds to the residual oxygen containing groups bonded to C and metal atoms, such as O═C–O (533.5 eV), H–O (531.7 eV), and O–Co/Fe (530.0 eV) (Fig. S8B, ESI†). A trace amount of Co and Fe elements (~1 atomic%) is detected by XPS, since most of them are encapsulated by the carbon layer. The Co $2p_{3/2}$ XPS spectrum is fitted into two peaks with the binding energies of 778.6 and 780.4 eV (Fig. S8C, ESI†), corresponding to Co(0) and Co(II,III), respectively. The peaks at the binding energies of 782.6 and 785.2 eV should be the satellite peaks of Co $2p_{3/2}$ peaks. The Fe $2p_{3/2}$ XPS spectrum can be divided into three peaks with the binding energies of 707.5, 710.1, and 712.2 eV (Fig. S8D, ESI†), which should be ascribed to Fe(0), Fe(II), and Fe(III), respectively. The peaks belonging to Co(II,III) and Fe(II,III) emerge due to the surface oxidation of Co and Fe nanoparticles.

To assess the ORR catalytic activity, cyclic voltammetry (CV) and linear sweep voltammogram (LSV) measurements are performed on a rotating disk electrode (RDE). The ORR catalytic activity is firstly investigated by CV measurements in N_2 and O_2-saturated 0.1 M KOH electrolytes (Fig. S9, ESI†). The voltammetric response of the (Fe,Co) NCs in N_2-saturated solution showed a featureless curve, without the typical peaks associated with iron and cobalt-containing species. While an ORR peak with the peak potential of 0.84 V is obviously seen in the CV curve measured in the O_2-saturated electrolyte. The

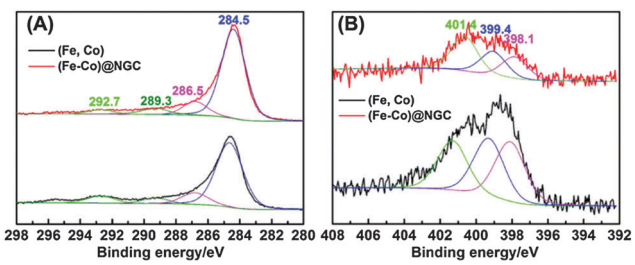

Fig. 2 (A) The C 1s and (B) N 1s XPS spectra of the (Fe,Co) and (Fe,Co)@NGC NCs.

LSV curves for equal mass electrode materials ($\sim$0.4 mg cm^{-2}) are measured to compare the ORR catalytic activity. Fig. 3A shows the LSV curves of the (Fe,Co) NC catalysts transformed from the $Fe_3[Co(CN)_6]_2$ NCs in the temperature range of 600–900 °C. The (Fe,Co) NCs catalyst formed at 700 °C achieves the maximum ORR catalytic activity with the onset (E_{onset}) and half-wave ($E_{1/2}$) potentials of 0.88 and 0.80 V. Its catalytic activity is also better than that of the monometallic Fe and Co catalysts (Fig. 3B and C), revealing that Fe and Co at the interface of carbon enhance ORR catalytic activity. Introducing the NGC shell into the (Fe,Co) NCs further improves ORR catalytic activity with the E_{onset} and $E_{1/2}$ of 0.91 and 0.85 V (Fig. 3B), which are well comparable to that of the Pt/C catalyst (Fig. 3B and C).

A rotating ring-disk electrode (RRDE) was employed to investigate the ORR kinetics. The percentage of peroxide species with respect to the total oxygen reduction products and the electron transfer number (n) are calculated from RRDE curves according to eqn (S4) and (S5) in the experimental section (ESI†), and the results are shown in Fig. 3D. The yield of peroxide species for the (Fe,Co)@NGC NC catalyst is obviously lower than that for the (Fe,Co) NCs catalyst ($>$23%), and close to that for the Pt/C catalyst over the measured potential range. The n of up to $\sim$3.7 can be achieved for the (Fe,Co)@NGC NC catalyst in the limiting current region (0.4–0.6 V *vs.* RHE). Analogously, the n determined from the Koutecky–Levich (K–L) plots is approximately 3.8 for the (Fe,Co)@NGC NCs catalyst in the potential range of 0.4–0.6 V *vs.* RHE (Fig. S10, ESI†), which is consistent with the results based on the RRDE analysis. Thus, the ORR process under the catalysis of the (Fe,Co)@NGC NCs is mainly *via* a four electron (4e) pathway.

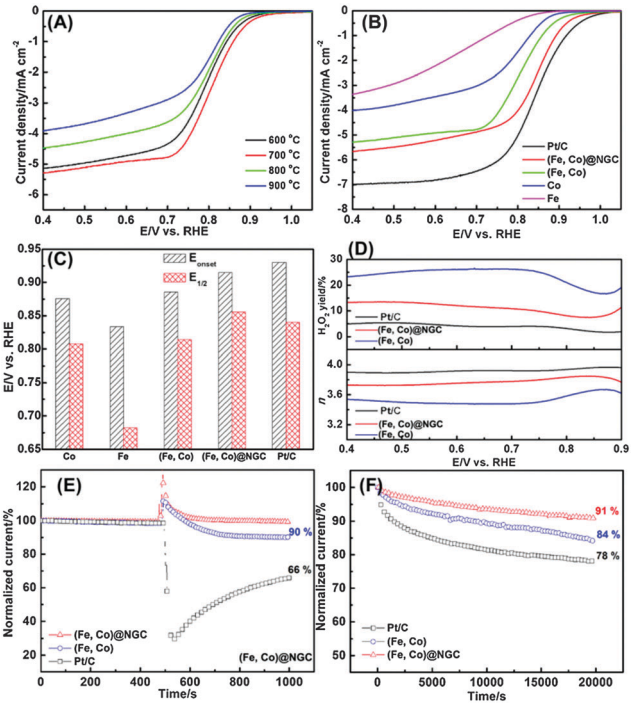

Fig. 3 (A, B) Linear scan voltammogram (LSV) curves of the (Fe,Co) NCs thermally decomposed at various temperatures in O_2-saturated 0.1 M KOH at a scan rate of 5 mV s^{-1} and a rotating rate of 2400 rpm. (B) LSV curves of the Fe, Co, (Fe,Co), (Fe,Co)@NGC, and Pt/C catalysts in O_2-saturated 0.1 M KOH at a scan rate of 5 mV s^{-1} and a rotating rate of 2400 rpm. (C) The corresponding onset (E_{onset}) and half-wave ($E_{1/2}$) potentials of the Fe, Co, (Fe,Co), (Fe,Co)@NGC and Pt/C catalysts. (D) The peroxide yield (top) and electron transfer number (n) of the (Fe,Co), (Fe,Co)@NGC, and Pt/C catalysts at various potentials calculated from the RRDE data. (E) Chronoamperometric responses at 0.50 V *versus* RHE reference electrode at a rotating rate of 2400 rpm in O_2-saturated 0.1 M KOH and methanol (20 vol%) electrolyte. (F) Chronoamperometric responses at 0.50 V *versus* RHE reference electrode in the O_2-saturated 0.1 M KOH electrolyte at a rotating rate of 2400 rpm.

The Tafel plots shown in Fig. S11 (ESI†) can give some hints to elucidate the ORR mechanism. The Fe and Co catalysts exhibit a similar Tafel slope ($\sim$64 mV dec^{-1}) at low overpotential, indicating that they share the same ORR mechanism, which is close to $\sim 2.303RT/F$ (59 mV dec^{-1}) due to the adsorption isotherm of the oxygenated species (Temkin behaviour). While they have different exchange current densities, which should be ascribed to different M–N–C (M = Co, Fe) active centers.[11] The Tafel slopes of up to 86 and 78 mV dec^{-1} are achieved on the (Fe,Co) and (Fe,Co)@NGC catalyst, respectively, which share a similar ORR mechanism with the Pt/C catalyst (82 mV dec^{-1}). Thus, the protonation of O^{2-} on the active sites of catalysts is the main rate-determining step.[2]

The crossover effect and stability are also the vital factors related to the catalytic performance. To investigate possible crossover effects,[20] we have investigated the electrocatalytic selectivity of the (Fe,Co)@NGC NCs catalyst against the electrooxidation of methanol molecules. The ORR current for the (Fe,Co)@NGC NCs catalyst almost shows no change with the addition of methanol, while there is $\sim$10% and 34% of loss for the (Fe,Co) NCs and Pt/C catalyst, respectively (Fig. 3E), suggesting a great tolerance for methanol molecules. The good crossover effect for methanol molecules can also be seen from the LSV curves before and after the addition of methanol molecules, in which there is no noticeable change for E_{onset}, and only $\sim$14 mV decrease for $E_{1/2}$ (Fig. S12, ESI†). Moreover, the excellent cycling stability of the (Fe,Co)@NGC NCs catalyst is demonstrated, which is assessed using chronoamperometric (CA) measurements. As depicted in Fig. 3F, the ORR current produced in the (Fe,Co)@NGC catalyst is lost only by $\sim$9% over 20 000 s of continuous operation, while the (Fe,Co) NCs and Pt/C catalyst exhibit $\sim$16% and 22% decreases in the ORR current tested under the same conditions, respectively. It is also better than that of the Fe_3C@C/graphene catalyst derived from PB NCs (8.2% decrease in the current density within 6000 s).[2] After 5000 repetitive cycles in the potential range of 1.1–0.4 V, the E_{onset} and $E_{1/2}$ on the (Fe,Co)@NGC NC catalyst decrease only by 15 and 20 mV, respectively (Fig. S13, ESI†). The stability even surpasses that of the graphitic layer-encapsulated Fe_3C catalyst (22 mV after 4500 cycles).[4] Thus, such an excellent crossover effect and stability should be mainly ascribed to the NGC shell deposited at the surface of (Fe,Co) NCs as a protective layer, just like the graphitic layer in the Fe_3C/C hollow sphere catalyst.

In conclusion, we have developed a facile approach to synthesize a new type of core–shell structured (Fe,Co)@NGC NCs catalyst derived from $Fe_3[Co(CN)_6]_2$@PDA NCs at a low

temperature of 700 °C. Introducing NGC at the surface of (Fe,Co) NCs as a protective layer does not influence the ORR mechanism and cooperatively enhances catalytic activity. More importantly, it significantly improves the crossover effect and catalytic stability performance. Therefore, we believe that this work can inspire the research on the rational design of the structure and component of highly efficient non-precious electrocatalysts, to replace precious metal catalysts for energy conversion application.

Notes and references

1 Y. Liang, Y. Li, H. Wang, J. Zhou, J. Wang, T. Regier and H. Dai, *Nat. Mater.*, 2011, **10**, 780; J. Suntivich, H. A. Gasteiger, N. Yabuuchi, H. Nakanishi, J. B. Goodenough and Y. Shao-Horn, *Nat. Chem.*, 2011, **3**, 546.
2 Y. Hou, T. Huang, Z. Wen, S. Mao, S. Cui and J. Chen, *Adv. Energy Mater.*, 2014, **4**, 1400337.
3 Y. Hu, J. O. Jensen, W. Zhang, Y. J. Huang, L. N. Cleemann, W. Xing, N. J. Bjerrum and Q. F. Li, *ChemSusChem*, 2014, **7**, 2099.
4 Y. Hu, J. O. Jensen, W. Zhang, L. N. Cleemann, W. Xing, N. J. Bjerrum and Q. Li, *Angew. Chem., Int. Ed.*, 2014, **53**, 3675.
5 K. P. Gong, F. Du, Z. H. Xia, M. Durstock and L. M. Dai, *Science*, 2009, **323**, 760.
6 Y. Meng, D. Voiry, A. Goswami, X. Zou, X. Huang, M. Chhowalla, Z. Liu and T. Asefa, *J. Am. Chem. Soc.*, 2014, **136**, 13554; Y. Zhao, L. Yang, S. Chen, X. Wang, Y. Ma, Q. Wu, Y. Jiang, W. Qian and Z. Hu, *J. Am. Chem. Soc.*, 2013, **135**, 1201; J. Shui, M. Wang, F. Du and L. Dai, *Sci. Adv.*, DOI: 10.1126/sciadv.1400129.
7 G. Wu, K. L. More, C. M. Johnston and P. Zelenay, *Science*, 2011, **332**, 443; M. Lefevre, E. Proietti, F. Jaouen and J. P. Dodelet, *Science*, 2009, **324**, 71; J. Tian, A. Morozan, M. T. Sougrati, M. Lefevre, R. Chenitz, J. P. Dodelet, D. Jones and F. Jaouen, *Angew. Chem., Int. Ed.*, 2013, **52**, 1.
8 B. Winther-Jensen, O. Winther-Jensen, M. Forsyth and D. R. MacFarlane, *Science*, 2008, **321**, 671.
9 J.-S. Lee, G. S. Park, S. T. Kim, M. Liu and J. Cho, *Angew. Chem., Int. Ed.*, 2013, **52**, 1026; H. T. Chung, J. H. Won and P. Zelenay, *Nat. Commun.*, 2013, **4**, 5; J. Liang, R. F. Zhou, X. M. Chen, Y. H. Tang and S. Z. Qiao, *Adv. Mater.*, 2014, **26**, 6074; D. H. Lee, W. J. Lee, W. J. Lee, S. O. Kim and Y.-H. Kim, *Phys. Rev. Lett.*, 2011, 106; Z.-S. Wu, L. Chen, J. Liu, K. Parvez, H. Liang, J. Shu, H. Sachdev, R. Graf, X. Feng and K. Muellen, *Adv. Mater.*, 2014, **26**, 1450; Z. Xiang, Y. Xue, D. Cao, L. Huang, J.-F. Chen and L. Dai, *Angew. Chem., Int. Ed.*, 2014, **53**, 2433; Z. Wen, S. Ci, F. Zhang, X. Feng, S. Cui, S. Mao, S. Luo, Z. He and J. Chen, *Adv. Mater.*, 2012, **24**, 1399.
10 J. Sanetuntikul and S. Shanmugam, *Electrochim. Acta*, 2014, **119**, 92; L. Hu, R. Zhang, L. Wei, F. Zhang and Q. Chen, *Nanoscale*, 2015, **7**, 450.
11 R. Zhou and S. Z. Qiao, *Chem. Commun.*, 2015, **51**, 7516.
12 D. Deng, L. Yu, X. Chen, G. Wang, L. Jin, X. Pan, J. Deng, G. Sun and X. Bao, *Angew. Chem., Int. Ed.*, 2013, **52**, 371; F. Zhang, X. Pan, Y. Hu, L. Yu, X. Chen, P. Jiang, H. Zhang, S. Deng, J. Zhang, T. B. Bolin, S. Zhang, Y. Huang and X. Bao, *Proc. Natl. Acad. Sci. U. S. A.*, 2013, **110**, 14861.
13 R. O. Grisdale, *J. Appl. Phys.*, 1953, **24**, 1288.
14 A. S. Klymchenko, S. Furukawa, K. Muellen, M. Van der Auweraer and S. De Feyter, *Nano Lett.*, 2007, **7**, 791.
15 X. Wang, L. Zhi, N. Tsao, Z. Tomovic, J. Li and K. Muellen, *Angew. Chem., Int. Ed.*, 2008, **47**, 2990.
16 T. Palaniselvam, B. P. Biswal, R. Banerjee and S. Kurungot, *Chem. – Eur. J.*, 2013, **19**, 9335.
17 K. Ai, Y. Liu, C. Ruan, L. Lu and G. Lu, *Adv. Mater.*, 2013, **25**, 998.
18 S. U. Yu, Y. Cho, B. Park, N. Kim, I. S. Youn, M. Son, J. K. Kim, H. C. Choi and K. S. Kim, *Chem. Commun.*, 2013, **49**, 5474.
19 K. Haubner, J. Murawski, P. Olk, L. M. Eng, C. Ziegler, B. Adolphi and E. Jaehne, *ChemPhysChem*, 2010, **11**, 2131; A. Ganguly, S. Sharma, P. Papakonstantinou and J. Hamilton, *J. Phys. Chem. C*, 2011, **115**, 17009.
20 A. Heinzel and V. M. Barragan, *J. Power Sources*, 1999, **84**, 70.

